LA-UR- 09-05853

Approved for public release;
distribution is unlimited.

Title:	The Guderley Problem Revisited
Author(s):	Scott D. Ramsey, X-3-V James R. Kamm, X-3-V John H. Bolstad
Intended for:	Submission to the Journal "Shock Waves"

Form 836 (7/06)

Noname manuscript No.
(will be inserted by the editor)

The Guderley Problem Revisited

Scott D. Ramsey · James R. Kamm · John H. Bolstad

Received: date / Accepted: date

Abstract The self-similar converging-diverging shock wave problem introduced by Guderley in 1942 has been the source of numerous investigations since its publication. In this paper, we review the simplifications and group invariance properties that lead to a self-similar formulation of this problem from the compressible flow equations for a polytropic gas. The complete solution to the self-similar problem reduces to two coupled nonlinear eigenvalue problems: the eigenvalue of the first is the so-called similarity exponent for the converging flow, and that of the second is a trajectory multiplier for the diverging regime. We provide a clear exposition concerning the reflected shock configuration. Additionally, we introduce a new approximation for the similarity exponent, which we compare with other estimates and numerically computed values. Lastly, we use the Guderley problem as the basis of a quantitative verification analysis of a cell-centered, finite volume, Eulerian compressible flow algorithm.

Keywords Compressible flow · Exact solution · Convergent flow · Code verification

PACS 02.20.Qs · 47.10.A · 47.11.Df · 47.40.Nm

Mathematics Subject Classification (2000) 65Z05 · 76N15 · 76L05 · 70G65

1 Introduction

The problem of a strong shock wave converging cylindrically or spherically in a gas is well known in hydrodynamics and is considered important in varied contexts. For example, the problem of converging compressible flow is familiar to the laser fusion

S. Ramsey
Los Alamos National Laboratory, Los Alamos, NM 87545 USA
Tel.: +1-505-665-8930
Fax: +1-505-665-7725
E-mail: ramsey@lanl.gov

J. Kamm
Los Alamos National Laboratory, Los Alamos, NM 87545 USA

J. Bolstad
Consultant, Livermore, CA 94550 USA

community [2,16,46,58] as well as in astrophysical contexts, e.g., in double-detonation supernovae [21].

Guderley was the first to investigate the basic problem of a strong cylindrically or spherically symmetric shock wave converging into an inviscid, non-radiating, non-heat-conducting, perfect gas [24] (though this particular problem was also solved independently by Landau and Stanyukovich in 1944 [60]). Guderley recognized that certain physical assumptions lead to a self-similar problem formulation. The solution of the self-similar problem is contingent upon the determination of the numerical value of a so-called "similarity exponent" that characterizes the space-time path of the infinite-strength incoming (converging) and finite-strength reflected (diverging) shock waves in proximity to the location of collapse. In the years following Guderley's seminal work, various authors including Butler [11], Lazarus and Richtmyer [38], Lazarus [36], and Hafner [28] calculated the numerical value of this similarity exponent (a function of the adiabatic exponent and geometry) to several significant figures using various techniques.

The "classic" Guderley problem, also reviewed by Meyer-ter-Vehn and Schalk [41], has variations that have been explored in some detail. Axford and Holm [4] used group theoretic techniques to determine the general equation of state (represented through the adiabatic bulk modulus) that admits self-similar solutions for a Guderley-type problem. Wu and Roberts [66] investigated the special case of a strong shock wave converging into a Van der Waals gas, and various authors have found similarity solutions for strong shock waves converging into dusty gases [33], variable-density gases [40,62], and radiating gases [30,48]. Additionally, Axford and Holm [5] explored a quasi-self-similar solution regime for finite-strength shocks, Ponchaut et al. [52,53] also relaxed Guderley's original strong shock assumption, and Hornung et al. [32] considered the universality of imploding shock solutions from examination of approximate solutions for the Guderley problem and computed solutions of converging shocked flows. The stability of Guderley flows was first investigated by Morawetz [45] and subsequently discussed by Häfele [26], Axford and Holm [4], Brushlinskii [10], and, recently, Clarisse [15].

Consistent with the assumptions motivating the governing Euler equations of inviscid, non-heat-conducting, compressible flow, the converging shock wave reflects through the origin, resulting in a diverging shock wave immediately following focus. It is easily proven that the similarity exponent governing the trajectory of the reflected shock is the same as that determined for the incoming case; consequently, many authors do not address reflection. Some authors, such as Lazarus and Richtmyer [38], Fernández [20], Lazarus [36], Rodríguez and Amable [56], Wu and Roberts [66], Bilbao and Gratton [7], and Ponchaut [52], engage in discussions describing the flow into and out of the reflected shock wave.

In fact, the reflected portion of Guderley's converging shock wave problem constitutes a separate eigenvalue problem. In addition to the similarity exponent determined as part of the analysis of the converging portion, an *a priori* unknown trajectory multiplier must be determined in order to fully realize the (scale-invariant) physical flow variables. In general, this multiplier is determined numerically through integration of the reduced flow equations on either side of the reflected shock, supplemented by boundary condition matching; this is achieved thorough the satisfaction of the generalized Rankine-Hugoniot jump conditions at a certain point in similarity variable space. The evaluation of this multiplier is subtle: we present a thorough treatment for the sake of increased clarity and understanding.

One objective of this work is to rigorously examine both the converging and diverging portions of Guderley's original problem. We present a reduction of the one-dimensional inviscid flow equations to self-similar form based on Lie Group techniques in the spirit of the work of Coggeshall et al. [19,17,18], as opposed to ansatz or dimensional arguments[1]. Additionally, a number of existing approximations to the value of the similary exponent are summarized, and a new approximation based upon the work of Hirschler and Gretler [31] (H&G) is introduced. We focus only on the determination of standard solution modes (i.e., not those implied to exist by Lazarus and Richtmyer [38] and by Lazarus [36], and discussed in further detail by Van Dyke and Guttmann [63]). A description of the numerical solution of the problem as a whole will follow the analytic and semi-analytic considerations.

The structure of this paper is as follows. In §2 we provide a brief review of the Guderley problem. The presentation in §3 describes how this problem is reduced to its self-similar form for both the converging-shock and reflected-shock phases. We discuss various approximations of the critical similarity exponent (including our new contribution) in §4. Comparisons of compressible flow code simulations of the Guderley problem with the semi-analytic ("exact") solution are given in §5, including quantitative verification analysis of an Eulerian finite-volume code. We conclude in §6.

2 Review of the Guderley Problem

The "classical Guderley problem" begins with the consideration of an infinitely strong, symmetric shock wave focusing perfectly on an infinite axis (cylindrical geometry) or point (spherical geometry). The source of the shock wave is not discussed in this scenario, but the initial state of the gas into which the wave is propagating is well-defined. Denoting physical flow variables in this unshocked region by the subscript 0, the initial state is given by

$$u_0(r,t) = 0\,, \tag{1}$$

$$\rho_0(r,t) = \text{constant}\,, \tag{2}$$

$$P_0(r,t) = 0\,, \tag{3}$$

where r denotes position ($r \geq 0$), t time ($-\infty < t < 0$ for the converging mode, $0 < t < \infty$ for the reflected mode), u velocity, ρ mass density, and P material pressure. For a one-dimensional (1-D Cartesian, cylindrical, or spherical), smooth flow free of viscosity, heat conduction, radiation, and body forces, the Euler equations describe fluid motion at all continuous (i.e., non-shock) locations:

$$\frac{\partial \rho}{\partial t} + \frac{\partial (\rho\, u)}{\partial r} + (m-1)\,\frac{\rho\, u}{r} = 0\,, \tag{4}$$

$$\frac{\partial u}{\partial t} + u\,\frac{\partial u}{\partial r} + \frac{1}{\gamma}\left[\frac{c^2}{\rho}\,\frac{\partial \rho}{\partial r} + 2\,c\,\frac{\partial c}{\partial r}\right] = 0\,, \tag{5}$$

$$\frac{\partial c}{\partial t} + u\,\frac{\partial c}{\partial r} + (\gamma-1)\,c\left[\frac{\partial u}{\partial r} + \frac{(m-1)\,u}{r}\right] = 0\,, \tag{6}$$

[1] Dimensional analysis finds *only* scale-invariant variables and solutions, while application of Lie group techniques systematically identifies *all* invariant functions and solutions.

where c denotes the local sound speed, defined through the pressure and density by:

$$c^2 \equiv \gamma P/\rho . \tag{7}$$

Here we consider only a polytropic gas with the incomplete equation of state (EOS) given by:

$$P(\rho, e) = (\gamma - 1)\, \rho e , \tag{8}$$

where e is the specific internal energy (SIE). In (4–8), γ denotes the adiabatic exponent ($1 < \gamma < \infty$), and m the space dimension ($m = 1$, 2, or 3 for 1-D planar, cylindrical, or spherical symmetry). Equations (4–8) are not valid globally, though shock jump conditions are available to connect the pre-shock and post-shock flow fields. In particular, since the converging shock wave is assumed to be infinitely strong, the strong limit of the Rankine-Hugoniot jump conditions may be used to connect the flow just upstream to that just downstream:

$$\frac{\rho_{2a}}{\rho_0} = \frac{\gamma + 1}{\gamma - 1} , \tag{9}$$

$$u_{2a} = \frac{2}{\gamma - 1}\, \dot{R}_s^-(t) , \tag{10}$$

$$P_{2a} = \frac{2}{\gamma - 1}\, \rho_0 \left[\dot{R}_s^-(t)\right]^2 , \tag{11}$$

where the subscript $2a$ denotes the state just upstream of (behind) the converging shock, and $\dot{R}_s^-(t)$ denotes the converging shock speed.

Equations (9–11) are valid for all $t < 0$ (the convergent mode). After shock focus and subsequent reflection about the axis or point of symmetry (analogous to reflection from a rigid wall in 1-D planar symmetry), these equations cease to be valid. As the strength of the reflected shock wave for $t > 0$ is unknown (due to the fact that the pressure field downstream (ahead) of the reflected shock wave is once-disturbed and not necessarily negligible), general jump conditions must be employed to connect the flow in the post-reflection space-time regions. After some manipulation, the standard Rankine-Hugoniot jump conditions in this case can be written as [24]:

$$\rho_3 = \rho_{2b}\, \frac{\gamma + 1}{\gamma - 1 + 2\left[c_{2b}/\left(u_{2b} - \dot{R}_s^+(t)\right)\right]^2} , \tag{12}$$

$$u_3 = \dot{R}_s^+(t) + \frac{1}{\gamma + 1}\left[u_{2b} - \dot{R}_s^+(t)\right]\left\{\gamma - 1 + 2\left(\frac{c_{2b}}{u_{2b} - \dot{R}_s^+(t)}\right)^2\right\} , \tag{13}$$

$$P_3 = P_{2b} + \frac{2}{\gamma + 1}\, \rho_{2b}\left[u_{2b} - \dot{R}_s^+(t)\right]^2 \left\{1 - \left(\frac{c_{2b}}{u_{2b} - \dot{R}_s^+(t)}\right)^2\right\} , \tag{14}$$

where the subscripts $2b$ and 3 denote, respectively, the states just downstream and upstream of the reflected shock, and $\dot{R}_s^+(t)$ denotes the reflected shock speed. Additional constraints apply at $r = 0$ for $t > 0$:

$$|\rho_3(0,t)| < \infty , \tag{15}$$

$$u_3(0,t) = 0 , \tag{16}$$

$$|P_3(0,t)| < \infty . \tag{17}$$

In principle, and in conjunction with the conditions that the flow field be single-valued for all t (including $t = 0$ but excepting shock wave positions) and bounded as $r \to \infty$ for $t \neq 0$, (1–17) are sufficient to fully determine the flow field surrounding both the converging and reflected shock waves for all t.

3 Semi-Analytic Evaluation of the Guderley Solution

Following from group theoretic considerations of (4–6)[2], the following change of variables may be derived:

$$\xi \equiv \mathrm{sgn}(t)\,\frac{r}{|t|^{\alpha}}\,, \tag{18}$$

$$u(r,t) \equiv \frac{r}{t}\,V(\xi)\,, \tag{19}$$

$$c^2(r,t) \equiv \frac{r^2}{t^2}\,C(\xi)\,, \tag{20}$$

$$\rho(r,t) \equiv \rho_0\,D(\xi)\,, \tag{21}$$

where α is a dimensionless constant referred to as the similarity exponent. We utilize this choice of variables and follow the particularly clear development of Chisnell [14]. Lazarus [36] takes a different approach, using as his fundamental nondimensional independent variable a quantity proportional to $\xi^{-1/\alpha}$. This choice of variables has implications in the computational evaluation of the solution, as we discuss in §§3.1 and 3.2 and Appendix B.

Analogs of (4–6) may be transformed to a system of ordinary differential equations (ODEs) in the dimensionless variables ξ, $D(\xi)$, $V(\xi)$, and $C(\xi)$:

$$\frac{1}{C}\,\frac{dC}{dV} = \frac{2\,\Delta\,\{1 + \{[(1-\alpha)/[\gamma\,(\alpha - V)]]\}\} + (\gamma - 1)\,Q(V)}{\Delta\,\{m\,V - [2\,(1-\alpha)/\gamma]\} + (\alpha - V)\,Q(V)}\,, \tag{22}$$

$$\frac{1}{D}\,\frac{dD}{dV} = \frac{Q(V) - \Delta\,\{[2\,(1-\alpha)]/[\gamma\,(\alpha - V)]\}}{(\alpha - V)\,Q(V) + \Delta\,\{m\,V - [2\,(1-\alpha)/\gamma]\}}\,, \tag{23}$$

$$\frac{1}{\xi}\,\frac{d\xi}{dV} = \frac{-\Delta}{(\alpha - V)\,Q(V) + \Delta\,\{m\,V - [2\,(1-\alpha)/\gamma]\}}\,, \tag{24}$$

where

$$\Delta \equiv -C + (V - \alpha)^2\,, \tag{25}$$

$$Q(V) \equiv m\,V\,(V - \alpha) + \frac{2\,(1-\alpha)}{\gamma}\,(\alpha - V) - V\,(V - 1)\,. \tag{26}$$

One can similarly transform (9–11), (12–14), (15–17), and the conditions that the flow field be single-valued for all t and bounded as $r \to \infty$ for $t \neq 0$, as these relations are invariant under the same group of point transformations as (4–6). Transformation of these expressions results in the following relations. At the incoming shock location:

$$D(\xi = -1) = \frac{\gamma + 1}{\gamma - 1}\,, \tag{27}$$

$$V(\xi = -1) = \frac{2\,\alpha}{\gamma + 1}\,, \tag{28}$$

$$C(\xi = -1) = \frac{2\,(\gamma - 1)\,\alpha^2}{(\gamma + 1)^2}\,. \tag{29}$$

[2] See Appendix A for a brief motivation and discussion.

As $t \to 0^-$:

$$D(\xi \to -\infty) = \text{constant}\,, \tag{30}$$

$$V(\xi \to -\infty) = 0\,, \tag{31}$$

$$C(\xi \to -\infty) = 0\,. \tag{32}$$

At the reflected shock (where $\xi \equiv \xi_R$):

$$D_3(\xi_R) = D_{2b}(\xi_R)\,\frac{\gamma+1}{\gamma-1+2\,[C_{2b}(\xi_R)/(V_{2b}(\xi_R)-\alpha)^2]}\,, \tag{33}$$

$$V_3(\xi_R) = \alpha + \frac{1}{\gamma+1}\,[V_{2b}(\xi_R)-\alpha]\,\left\{\gamma-1+2\,\left[C_{2b}(\xi_R)/(V_{2b}(\xi_R)-\alpha)^2\right]\right\}\,, \tag{34}$$

$$C_3(\xi_R) = \frac{1}{\gamma+1}\,\left\{\gamma-1+2\,\left[C_{2b}(\xi_R)/(V_{2b}(\xi_R)-\alpha)^2\right]\right\} \times \left\{C_{2b}(\xi_R) + \frac{2\gamma}{\gamma+1}\,[V_{2b}(\xi_R)-\alpha]^2\,\left\{1-\left[\frac{C_{2b}(\xi_R)}{(V_{2b}(\xi_R)-\alpha)^2}\right]\right\}\right\}\,. \tag{35}$$

As $r \to 0$ for $t > 0$:

$$|D(\xi=0)| < \infty\,, \tag{36}$$

$$V(\xi=0) = \text{constant}\,, \tag{37}$$

$$C(\xi=0) \to \infty\,. \tag{38}$$

Through the focus:

$$D_{2a}(\xi \to -\infty) = D_{2b}(\xi \to \infty)\,, \tag{39}$$

$$\lim_{t\to 0^+}\frac{r}{t}\,[V_{2a}(\xi(r,t)) - V_{2b}(\xi(r,t))] = 0\,, \tag{40}$$

$$\lim_{t\to 0^+}\frac{r^2}{t^2}\,[C_{2a}(\xi(r,t)) - C_{2b}(\xi(r,t))] = 0\,. \tag{41}$$

Together, (22–24) and (27–41) provide a framework for the Guderley problem in terms of ODEs and additional constraints. Different forms of these governing equations have been previously derived by various authors [14,36,38].

3.1 The Converging Shock

The calculation of the similarity exponent and evaluation of the numerical solution of (22–24) are carried out simultaneously, first using successive estimates for α and the initial and boundary conditions given by (27–29) and (30–32). With an initial estimate for α, numerical integration of (22–24) is typically started at the incoming shock represented by (27–29) and carried through to the state represented by (30–32). Between these states, however, the governing equations become singular when $\Delta = 0$. As shown by Chisnell [14], to remove the physically unrealistic singular behavior, it becomes necessary to impose the constraint:

$$Q(V^*) = m\,V^*\left(V^*-\alpha\right) + \frac{2\,(1-\alpha)}{\gamma}\,\left(\alpha - V^*\right) - V^*\left(V^*-1\right) = 0 \quad \text{when } \Delta = 0\,, \tag{42}$$

Table 1 Selected values of the similarity exponent α

	Cylindrical Geometry ($m = 2$)		Spherical Geometry ($m = 3$)	
γ	New value	Lazarus [36] $1/\lambda_{\text{std}}$	New value	Lazarus [36] $1/\lambda_{\text{std}}$
1.4	0.835323192	0.8353231919	0.717174501	0.7171745015
5/3	0.815624901	0.8156249014	0.688376823	0.6883768229
2	0.800112351	0.8001123512	0.667046070	0.6670460703
3	0.775666619	0.7756666194	0.636410594	0.6364105940
6	0.751561684	0.7515616841	0.610339148	0.6103391480

where V^* represents the V-coordinate of the $\Delta = 0$ singularity. Accordingly, the constraint given by (42) provides the means by which to remove this singularity and numerically determine a precise value for the similarity exponent. Concomitantly, the apparent singularity in (22–24) becomes integrable, and the numerical solution of these equations may be carried through to the state given by (30–32).

In the current work, this procedure was implemented using the equations based on the nondimensionalization of Lazarus [36].[3] We use the Netlib routines ODE to solve the system of differential equations and the one-dimensional rootfinder ZEROIN for determining the similarity exponent [22,47]. In the literature [28,31,36,38], there has been inconsistent reproduction of similarity exponent values beyond eight or nine decimal places, even for "standard" values of the adiabatic exponent. For $\gamma < 1.4$, accurate calculation of α becomes difficult, as discussed by Lazarus [36]. Even so, the results given in Table 1 are consistent with other published results.

3.2 The Reflected Shock

The converging shock wave solution mode is valid until focus ($t = 0$). At that time, the shock wave reflects about the point or axis of symmetry and proceeds to diverge outwards into the once-perturbed fluid with an unknown trajectory given by:

$$R_s^+(t) = B\,t^\beta\,, \tag{43}$$

where the parameters B and β are initially unknown, though it is easily shown that $\beta = \alpha$. The parameter B, however, requires more effort to calculate.

As the structure of the equations governing the flow for $t > 0$ has not changed (they are in fact given by (22–24)), numerical evaluation of the solution may, with a suitable change of variables (see Lazarus [36]), be continued beyond the state represented by (30–32) by means of two integrations. The first integration represents recovery of flow data beginning at $r \to \infty$ for all $t > 0$, and can be continued "inward" until the reflected shock wave is reached. Being coupled to the unknown value of B, the phase-space point corresponding to the reflected shock wave is unknown. If this location were known, then the general-strength Rankine-Hugoniot jump conditions would be applied there, and the integration of (22–24) could be continued to a suitable endpoint, namely, until (36–38) are satisfied. This final state represents the position $r = 0$ for $t > 0$.

To determine the phase space location of the reflected shock wave, Lazarus [36] devised a so-called "jump locus" methodology. A locus of "jump points" is formed by

[3] In Appendix B, we present the reasons for utilizing the Lazarus methodology in the numerical calculations together with computational details useful for practical implementations.

Table 2 Selected values of $B^{-\alpha}$, the reflected shock space-time location.

	Cylindrical Geometry ($m = 2$)		Spherical Geometry ($m = 3$)	
γ	New value	Lazarus [36,37]	New value	Lazarus [36,37]
1.4	2.815610935	2.815608	2.688492680	2.688492
5/3	1.694792696	1.694792	1.547894929	1.547896
2	1.199630409	1.199631	1.077253818	1.077255
3	0.763159927	0.763160	0.693969704	0.693970
6	0.540791267	0.5407906	0.531821969	0.5318222

applying the general Rankine-Hugoniot jump conditions to *every* numerical solution point beyond the state represented by (30–32), which corresponds to the origin in the (V, C)-plane. The numerical integration and resulting jump locus are continued to an arbitrary end point in the (V, C)-plane beyond the phase-space position corresponding to the reflected shock wave. The end point is determined by trial and error, subject to the success of the second numerical integration.

This second numerical integration follows the construction of the jump locus. It is subject to another appropriate change of variables and is initialized from (36–38). This integration is continued until a single intersection with the jump locus is obtained. Through this coupling, one identifies a unique phase-space point (on the jump locus) at which the reflected shock wave exists. Through suitable transformations of these results B is determined, and the entire diverging-phase solution can be constructed. Data from the first numerical integration beyond the location corresponding to the correct jump point are thereby rendered irrelevant; the same is true of the remainder of the jump locus. As for the converging shock calculation, in the current work our computational implementation of the reflected shock solution follows the Lazarus methodology.

Lazarus [36], defining his B as the reflected shock space-time location, published values of that parameter (found by taking B in (43) to the negative α power) in Tables 6.4–6.5 of that reference (subject to the erratum [37]).

For $\gamma < 1.4$, accurate calculation of $B^{-\alpha}$ becomes difficult, as discussed by Lazarus [36]. Even so, the results given in Table 2 are consistent with other published results.

4 Analytic Similarity Exponent Approximations

The nonlinear eigenvalue problem whose solution determines α has been solved approximately by a number of authors including Stanyukovich [60] and Chisnell [14]. A variety of physical and mathematical arguments exist so as to provide accurate estimates of the parameter α. We consider three approximations of α based on fundamental assumptions about the solution of the governing equations.[4] These estimates ultimately prove useful as first iterates or bracketing values on the true value of α, and are easily incorporated into numerical routines that iterate on the true value of the similarity

[4] These approximations are to be contrasted with the purely curve-fit approximation for α as a function of γ given by Hafner [27] for the spherical ($m = 3$) case:

$$\alpha = \left\{ [(\gamma - 1)/(2\,a)] + (1 - \alpha_\infty)^{-n} \right\}^{-1/n} + \alpha_\infty \,, \tag{44}$$

where $a = 3.26 \times 10^{-4}$, $n = 6$, and $\alpha_\infty = 0.375$.

exponent. It will be shown that for different ranges of γ and m, the relative accuracies of the approximations vary.

4.1 The Pressure Maximum Requirement

Stanyukovich [60] noted that for certain values of the adiabatic exponent, the pressure distribution behind the converging shock wave contains a single maximum. The existence of a pressure maximum in the flow behind a converging shock wave for arbitrary $\gamma > 1$ was dismissed by Zel'dovich and Raizer [68], but a work by Mishkin and Fujimoto (M&F) claimed otherwise [43,44]. Through this requirement, M&F derived an analytic expression for α claimed to be exact:

$$\alpha = \frac{\gamma + 2 + 2\sqrt{2\gamma}}{m\gamma + 2 + 2\sqrt{2\gamma}} \,. \tag{45}$$

The claim that (45) represents an exact solution for the similarity exponent was later refuted in papers by Lazarus [35] (with a rejoinder by Mishkin [42]) and Yousaf [67]; see also the paper by Wang [64]. This so-called "Landau-Stanyukovich rule" has also been recently extended by Gurovich and Fel [25] in order to construct upper and lower bounds on the true value of the similarity exponent.

4.2 The CCW Method

The Chester-Chisnell-Whitham (CCW) method is based upon Chester's result for the motion of a shock wave in a channel with a small change in area [12]. Chisnell first integrated Chester's result for "freely propagating" symmetric shock waves [13], and Whitham produced an alternative derivation of Chisnell's result [65]. For the case of strong shock waves, the ultimate result is an analytic formula relating the similarity exponent to the adiabatic exponent and space dimension.

It was apparently first noted by Sedov [59] that in the neighborhood of $(V, C) = (0, 0)$, the solution of (22) has the following limiting behavior:

$$\lim_{V \to 0+} C(V) = A_2 \, V^2 \,, \tag{46}$$

where A_2 is a constant to be determined. Since (46) automatically satisfies the boundary condition imposed upon the solution curve $C(V)$ given by (31,32), only the initial conditions (28,29) remain to be utilized. In particular, imposing the latter on (46) allows for determination of the constant A_2, and (46) becomes

$$C(V) = \frac{1}{2} \gamma \, (\gamma - 1) \, V^2 \,. \tag{47}$$

This equation represents an approximate analytic expression for the solution curve $C(V)$ of (22). Together with the condition $\Delta = 0$ and one solution of (42), (47) provides:

$$\alpha = \frac{(\gamma + 2)\sqrt{\gamma - 1} + \gamma\sqrt{2\gamma}}{(m\gamma + 2)\sqrt{\gamma - 1} + \gamma\sqrt{2\gamma}} \,. \tag{48}$$

4.3 The New Method

Inspired by the mathematical development of the CCW method just presented and a pseudo-limiting form of (22) first derived by Hirschler and Gretler [31] (H&G), a different approximate expression for the similarity exponent can be derived. Through the use of H&G's asymptotic treatment of (22) and the initial condition given by (28,29), an approximate solution can be shown to hold near the singular point at $\Delta = 0$ [54,55]:

$$C(V) = \alpha\,(\gamma - 1)\,V + \frac{1}{2}\,(1 - \gamma)\,V^2\,. \tag{49}$$

When evaluated at the singular point, (49) closes a system of three nonlinear algebraic equations with the condition $\Delta = 0$ and one solution of (42). Solution of this system for α is given by

$$\alpha = \frac{\gamma\,(\gamma + 1) - (\gamma - 2)\,\sqrt{\gamma^2 - 1}}{[2 + \gamma\,(m - 2)]\,\sqrt{\gamma^2 - 1} - \gamma\,[\gamma\,(m - 2) - m]}\,. \tag{50}$$

Equation (50) provides an alternative to the M&F and CCW approximations as an analytic approximation to the similarity exponent.

4.4 Discussion of Results

Evaluation of (45), (48), and (50) for various values of γ and m appears in Tables 3 and 4. Several trends may be discerned from these data.

1. The M&F approximation underestimates α for all γ and m.
2. The CCW approximation overestimates α only for a small range, $1.1 < \gamma < 2$, for $m = 2$ and 3.
3. The new approximation overestimates α for $\gamma > 5/3$ for $m = 2$ and 3.
4. The CCW and new approximations are both more accurate than the M&F appoximation for nearly all γ and m.
5. The new approximation is more accurate than the CCW approximation only for very large γ for $m = 2$ and 3.

As discussed in §3.1, an exact value for the similarity exponent is obtained by removing the $\Delta = 0$ singularity crossed by the solution of (22–24). While all Guderley solutions employ this technique, an additional constraint is necessary in order to construct analytic approximations to α. We have found that the global approach of utilizing both the initial conditions (28–29) and asymptotic solutions of (22–24) provides analytic approximations that retain a high level of fidelity to exact semi-analytic solutions (e.g., the CCW and new approximations). The purely local M&F approximation, which employs the pressure maximum requirement (i.e. a solution of (42) but *not* (28–29)) proves less accurate. Therefore, we hypothesize that both the local-global nature and accuracy of the additional constraint largely determines the accuracy of the resulting analytic approximation.

Reasons for the accuracy difference between the CCW and new approximations for various choices of γ and m are not easily resolved. We hypothesize that the relative local accuracy of the approximate solutions provided by (47) and (49) varies explicitly with γ. Accordingly, the accuracy of analytic α calculations based upon the implementation of these approximate solutions is seen to vary in a like manner.

Table 3 Estimates of the similarity exponent α for selected values of the adiabatic exponent

	Cylindrical Geometry ($m = 2$)			
γ	Exact [36]	M&F (45)	CCW (48)	New (50)
1.1	0.88524806	0.84650762	0.88247182	0.87355000
1.4	0.83532320	0.82815001	0.83537259	0.82945717
5/3	0.81562490	0.81450188	0.81604351	0.81481482
1.8	0.80859994	0.80840329	0.80888426	0.80980869
2.0	0.80011235	0.8	0.8	0.80384758
3.0	0.77566662	0.76742346	0.77266101	0.78679656
5.0	0.75640105	0.72714208	0.74881559	0.77296156
10	0.74182593	0.67683841	0.72904957	0.76193475
100	0.72853594	0.56575410	0.70941536	0.75124381
∞	0.72704805	0.5	0.70710678	0.75

Table 4 Estimates of the similarity exponent α for selected values of the adiabatic exponent

	Spherical Geometry ($m = 3$)			
γ	Exact [36]	M&F (45)	CCW (48)	New (50)
1.1	0.79596980	0.73386494	0.78966404	0.77548938
1.4	0.71717450	0.70670310	0.71728743	0.70860899
5/3	0.68837682	0.68705455	0.68925126	0.6875
1.8	0.67855370	0.67842021	0.67909796	0.68040211
2.0	0.66704607	0.66666667	0.66666667	0.67202771
3.0	0.63641060	0.62261729	0.62954164	0.64852814
5.0	0.61522398	0.57126728	0.59848539	0.62994081
10	0.60104880	0.51153119	0.57362550	0.61542374
100	0.58950281	0.39446102	0.54968526	0.60159367
∞	0.58828929	0.33333333	0.54691816	0.6

5 Compressible Flow Code Results

With semi-analytic results for the classical Guderley problem available, a counterpart numerical simulation was conducted using the general compressible flow solver of the program RAGE [23]. This algorithm is a variant of the Lagrange+remap-style Eulerian solver, as described, e.g., by Benson [6]; we refer to [23] for further details. With the semi-analytic solution, we can quantitatively gauge the quality of the compressible flow algorithm for both the incoming converging flow as well as the outgoing reflected shock solution.

Initializing a Guderley-like scenario in a generalized compressible flow code must be performed carefully. Theoretically, the converging shock wave that characterizes the Guderley problem is created in an infinitely weak state at $r \to \infty$ and $t \to -\infty$. The shock wave then propagates inwards with increasing strength due to geometric effects. It is impossible to precisely initialize a compressible flow code with such a prescription. Ponchaut et al. [53] and Hornung et al. [32] initialize generalized Guderley-like compressible flow calculations as "spherical shock tubes," i.e. by "numerically removing a membrane" separating a small pressure/sound speed differential at some position far from the focal point. The simulation is then allowed to evolve such that a Guderley solution is approached asymptotically in the immediate neighborhood of the focal point.

To be ostensibly more faithful to Guderley's original solution [24], a different approach is employed in the current work. Specifically, the solution to the Guderley problem is calculated on a specified, finite domain, $0 \leq r \leq r_{\max}$, at a chosen time when the shock wave is "near" the position $r = 0$. This computed solution is used to evalute cell-averaged values on the uniform mesh of the 1D, spherically symmetric compressible flow code. This choice of initialization is applied over a finite spatial domain including the origin.

In the compressible flow code calculations, a reflecting boundary condition is specified at the far boundary at $r_{\max}$, resulting in the generation of a spurious, inward-propagating rarefaction wave. Estimates suggest that this rarefaction wave propagates at approximately the $u - c$ characteristic speed. This information is used to identify subsets of the computational domains, unpolluted by this spurious rarefaction, on which to make quantitative comparisons of the flow code results with the self-similar Guderley solution computed from the ODEs.

The semi-analytic solution is computed in spherical geometry ($m = 3$) for an adiabatic exponent $\gamma = 3$. At $t = -1$ the initial state is chosen so that the converging shock is exactly at $r = 1$ (which forms an exact computational-cell boundary in all computations). With these initial conditions, reflection occurs at the origin at $t = 0$.

The initial incoming-shock configuration is shown in Fig. 1, which depicts the density, velocity, SIE, and pressure as functions of radial position over the entire computational domain. In all results and figures, flow quantities are in consistent cgs units. The values shown are cell-centered, cell-averaged quantities on 1200 equally-spaced zones between $r = 0$ and $r_{\max} = 3$. This figure shows that the incoming (negative) velocity peaks at the shock, located at $r = 1$, as do the pressure and SIE. In the upstream vicinity of the shock, the density gradually decreases to its immediate post-shock value.[5]

The configuration of Fig. 1 is used as initial conditions for the compressible flow solver. The semi-analytic and computed density fields at $t = -0.5$, -0.1, 0.1, and 0.5, are shown in Figs. 2, 3, 4, and 5, respectively. These figures also contain plots of the pointwise error, $|\tilde{y}_j^E - \tilde{y}_j^C|$, in each of the computed solutions; here, $\tilde{y}_j$ represents the solution averaged over cell j for either the exact (E) or computed (C) solution. Corresponding plots of the velocity, SIE, and pressure fields are provided by Ramsey [55]. We now turn to a discussion of these results.

5.1 Start-Up Errors

A prominent feature of Figs. 2–5 is the "dip" in the computed density fields. This dip is seen to exist in the density solution field for all post-initialization times. Additionally, "bumps" appear in the SIE field (provided by Ramsey [55]) at positions corresponding to the density dips for given times. These dips and bumps appear to annihilate one another in the computed pressure field and are not particularly noticeable in velocity results [55]. Quantitative estimates suggest that the dips and bumps move in the fixed Eulerian frame at approximately the material speed.

Phenomena of this type are not unique to the Guderley problem. In particular, dips and bumps such as those observed in Figs. 2–5 appear even in simple 1D planar numerical calculations initialized with exact solutions involving shock waves. This

[5] Cell averages are determined from numerical integrations using conserved quantities. See Appendix C for a discussion.

phenomenon is discussed in detail by Arora and Roe [1]; see also LeVeque [39]. For the purposes of this investigation, it is sufficient to recognize that the density dips are generated by finite volume numerical shock-capturing algorithms. While it is reasonable to assume that details of this phenomenon vary with different compressible flow algorithms, to the authors' knowledge there is no evidence in the literature that this phenomenon can be eliminated in Eulerian finite-volume codes.

The magnitude of the start-up error remains approximately constant in time. The spatial extent of the error increases slightly from $t = -0.5$ to $t = -0.1$, but is then compressed at $t = 0.5$, presumably associated with the passage of the reflected shock. As suggested by Fig. 5, however, the presence of the startup error does little to affect either the position or strength of the reflected shock subsequent to its interaction with this feature.

Figures 4 and 5 suggest that the shock capturing algorithm numerically approximates well the shock focusing and subsequent reflection at the origin at $t = 0$, i.e., the flow features of the semi-analytic solution subsequent to focus are captured in the computed solution. For only the coarsest resolution does the calculated shock position deviate noticeably from the semi-analytic solution.

5.2 Effects of Initialization with a Post-Focus State

The presence of the post-shock errors near the origin lead us to question how the compressible flow algorithm would behave if initialized with a post-focus state. Using an initialization with a state subsequent to shock focusing time, we find the computed behavior to be more precise than with the converging flow initialization. More precisely, we evaluate the semi-analytic solution at a time ($t = 0.018594543$ for $m = 3$ and $\gamma = 3$) when the shock is located at $r = 0.1$, and use those values to initialize the compressible flow code. Figure 6 depicts the density, velocity, SIE, and pressure as functions of radial position over a subset of the computational domain. These values are cell-centered, cell-averaged quantities on 1200 equally-spaced zones between $r = 0$ and $r = 3$. This figure shows the strong peaks in pressure, velocity, and density behind the outgoing shock as it encounters the incoming flow.

Comparison between the computed results at $t = 0.5$ in Figs. 5 and 7 corresponding to the different initializations reveals two significant differences. The first difference is the near-origin behavior. Specifically, a choice of post-reflection initialization drastically reduces the near-origin error—a fact explained by the computed solution not being subject to the consequences of singular behavior at $t = 0$.

The second difference is the significant reduction (but not elimination) of the density start-up error in Fig. 7: a small, localized flow error is apparent in this figure between $r = 0.1$ and $r = 0.15$. We speculate that this feature has the same cause as the start-up error evident in Figs. 3–5. A possible explanation as to why this phenomenon has smaller amplitude and spatial extent is given by the different flow geometry of the two different initial conditions: the initialization at $t = -1$ corresponds to converging flow, while an initialization with a semi-analytic solution at any $t > 0$ (including that shown in Fig. 6) corresponds to diverging flow. We hypothesize that the divergent flow may reduce the start-up errors.

5.3 Verification Analysis

Code verification analysis is an approach for gathering quantitative evidence that software for the solution of discretized equations generates results consistent with the corresponding continuum equations, e.g., by examining the error order-of-accuracy of the numerical results. Verification analysis (reviewed, e.g., by Oberkampf et al. [50] and Roy [57]) is a vitally important aspect of both algorithm and software development. The Guderley problem presents an ideal configuration with which to perform code verification analysis for cylindrically or spherically symmetric, converging-then-diverging compressible flow of an ideal gas. Using both the semi-analytic ("exact") and numerical ("computed") Guderley solutions, we evalute the spatial convergence properties of the RAGE compressible flow algorithm.[6]

In particular, we take as axiomatic the standard error ansatz,

$$||y^E - y^C|| = A\,(\Delta r)^\sigma\,, \tag{51}$$

where the superscripts E and C refer to the exact and computed solutions, respectively, $||\cdot||$ represents an error norm evaluated over a specified domain, Δr is a characteristic mesh dimension (e.g., the cell size on a uniform grid), A is a prefactor, and σ is the convergence rate (e.g., $\sigma = 1$ for a first-order method). As is standard for analysis of compressible flows, we consider the L_1 norm only (see, e.g., the monograph of Bouchut [8]). We approximate the left side of (51) as

$$||y^E - y^C|| \approx \frac{1}{\mathcal{V}} \sum_{j=1}^{N_r} |\tilde{y}_j^E - \tilde{y}_j^C|\, d\mathcal{V}_j\,, \tag{52}$$

where $\tilde{y}_j$ represents the solution averaged over cell j for either the exact (E) or computed (C) solution, $d\mathcal{V}_j$ is the volume of the spherical shell element centered at r_j, N_r is the number of cells between the origin and $r = 2$, and $\mathcal{V}$ is the volume of the sphere of radius 2.

The ansatz in (51) implicitly assumes that the convergence is monotonic and the method is consistent, i.e., that there is no $O(1)$ error. Using a series of calculations at different mesh resolutions, it is straightforward to infer best-fit values for both A and σ, which we accomplish with a standard nonlinear least-squares technique, using software described by Hemez et al. [29] In all calculations, the domain over which the errors were evaluated was $0 < r < 2$, thus neutralizing the effects of spurious boundary-driven rarefaction waves, as discussed in §5.1.

Results of this analysis are catalogued for various times in Tables 5 and 6. Additionally, example plots corresponding to the two data sets given at $t = 0.5$ (converging and diverging initialization) are provided in Fig. 8; further results are given by Ramsey [55]. Results for convergent initialization are provided in the first four rows of the tables and the left plot in the figure; the last row and right plot show results for divergent initialization.

These results show that the L_1-norm convergence rate is approximately linear for times before focus, with the exception of the density field. For times following focus, the L_1-norm convergence rate is universally but only slightly sublinear. In all fields except density, the L_1-norm convergence rate also decreases as focus is approached.

[6] One can also evaluate the temporal and combined spatio-temporal convergence properties of compressible flow algorithms [34].

Table 5 Summary of L_1-norm convergence data

	Premultipliers A			
t	ρ	u	P	e
−0.5	0.1886	0.1003	0.0510	0.0146
−0.1	0.2636	0.0364	0.0593	0.0178
+0.1	0.3078	0.0630	0.2102	0.0278
+0.5	0.2584	0.0547	0.1024	0.0275
+0.5*	0.1780	0.0460	0.1243	0.0091

*Initialized at $t = +0.018594543$; others initialized at $t = -1$.

Table 6 Summary of L_1-norm convergence data

	Convergence Rates σ			
t	ρ	u	P	e
−0.5	0.8652	1.046	1.028	0.9906
−0.1	0.9061	0.9720	1.002	0.9518
+0.1	0.9125	0.9794	0.9358	0.9324
+0.5	0.8501	0.9362	0.8694	0.9401
+0.5*	0.9605	1.011	0.9695	0.9444

*Initialized at $t = +0.018594543$; others initialized at $t = -1$.

Additionally, for times after focus, the L_1-norm convergence rates decrease for all fields except SIE. The pressure and SIE convergence rates decrease through focus.

Comparison of the error plots in Fig. 8 confirms what is seen for the density in Figs. 5 and 7, viz., the absolute error is smaller for the reflected shock initialization; moreover, the convergence rate in this case is higher. We observe similar trends for each flow quantity except the SIE.

The behavior observed in Tables 5 and 6, and Fig. 8, allows for the construction of hypotheses regarding effects that may influence the various convergence rates. Prominent trends that may prove amenable to explanation are the following.

1. Decreases in convergence rates during the time-evolution of the convergent solution mode.
2. Decreases in convergence rates during the time-evolution of the diverging solution mode.
3. Decreases in convergence rates across focusing time.
4. The inapplicability of trends 1 and 3 to the density field.
5. A marked improvement in convergence rates for initialization at a post-focus time.

Trends 1, 2, and 3 have a common explanation. At focus time, the exact Guderley solution for the physical velocity, SIE, and pressure fields increases without bound at the shock. This phenomenon is not numerically realizable due to inherent numerical precision limitations, so errors accrue in both the semi-analytic solution and compressible flow code results near focus time. Trends 1 and 3 do not apply to the density field convergence rates, and, in fact, these rates exhibit opposite behavior. A phenomenon that could prove responsible for this counterintuitive behavior is the interaction between a prominent start-up error and the fact that the density field solution does not increase without bound in the vicinity of $t = 0$. Similar reasoning might explain behavior in the pressure field that does not agree with trends 1–4, as this variable is

connected to the density and SIE through the polytropic EOS. Trend 5 notes an improvement in all L_1-norm convergence rates for a positive choice of initialization time, in all cases reaching essentially linear levels. This effect is clearly due to improved near-origin behavior and start-up error reduction in this case.

6 Conclusion

We have provided a brief overview of the theoretical framework necessary to construct a semi-analytic solution to Guderley's imploding shock problem. A number of existing analytic approximations to the problem's key parameter—the so-called similarity exponent—have been summarized and a new approximation was introduced.

We used the semi-analytic solution to the Guderley problem to initialize a compressible flow code on a finite domain and conduct what may be the first rigorous code verification analysis of an Eulerian compressible flow code with the full Guderley solution. Despite the well-known start-up errors that the computed solutions exhibit, these results show near-linear spatial convergence in the L_1-norm for the converging solution mode, and sublinear spatial convergence in the L_1-norm for the subsequent diverging solution mode. When initialized with a post-focus flow state, the errors in the computed solutions are notably smaller and the convergence results are marginally better.

The Guderley problem provides an attractive alternative to two other widely-used compressible flow code test problems: the Noh problem [3,49] and the Sedov problem [59]. The Guderley problem's advantages lie in the fact that it includes no unphysical wall heating effects, and is capable of describing coupled converging and diverging flow. It will be of interest to use the Guderley problem to evaluate the properties of other compressible flow algorithms, as well as to investigate 2D cylindrically symmetric and 3D geometries. Despite being introduced over 65 years ago, the Guderley problem continues to provide challenges to the theoretical and computational fluid physics communities.

Appendix A: Derivation of Similarity Variables

Equations (18–21) may be derived from the group invariance properties of (4–6). Specifically, (4–6) have been found [3–5,51] to admit the group of point transformations with the generator:

$$\hat{U} = (a_2 + a_3)\, r \frac{\partial}{\partial r} + (a_1 + a_2 t) \frac{\partial}{\partial t} + a_3\, u \frac{\partial}{\partial u} + a_4\, P \frac{\partial}{\partial P} + (a_4 - 2a_3)\, \rho \frac{\partial}{\partial \rho}\,, \quad \text{(A1)}$$

where the parameters a_i ($i = 1, 2, 3, 4$) are arbitrary constants.

Equations. (4–6) can be reduced to ordinary differential equations by introducing the invariant functions of the group as the new independent and dependent variables. These functions are determined by solving

$$\hat{U}\, \Psi(r, t, u, \rho, P)\big|_{\Psi=0} = 0\,, \quad \text{(A2)}$$

where Ψ is an arbitrary function of its arguments. Equation (A2) is a linear, first order partial differential equation whose solution is is found by the method of characteristics.

The characteristic equations of (A2) are:

$$\frac{dr}{(a_3+a_2)\,r} = \frac{dt}{(a_1+a_2 t)} = \frac{du}{a_3 u} = \frac{dP}{a_4 P} = \frac{d\rho}{(a_4-2a_3)\,\rho}\,. \tag{A3}$$

Invariance of the initial conditions, boundary conditions, etc. (as given in (1–3), (9–11), (12–14), and (15–17)) requires the following constraints on the group parameters a_i, $i = 1, 2, 3, 4$:

$$a_4 - 2\,a_3 = 0\,, \tag{A4}$$

$$a_1 = 0\,, \tag{A5}$$

$$a_2 = 1\,, \tag{A6}$$

$$1 + a_3 = \alpha\,, \tag{A7}$$

where α is a parameter to be determined in the course of the analysis. Here, (A4) expresses the assumption of a uniform ambient medium, (A5) reflects that the start time is arbitrary, and (A6) indicates that the time variable is not being scaled. With $a_2 = 1$, (A7) specifies a scaling of the radial coordinate with the similarity exponent α.

With (A4–A7), (A3) becomes

$$\frac{dr}{\alpha r} = \frac{dt}{t} = \frac{du}{(\alpha-1)\,u} = \frac{dP}{2\,(\alpha-1)\,P} = \frac{d\rho}{0}\,, \tag{A8}$$

where the zero denominator in the last term reflects the assumption of a uniform ambient medium, as expressed in (A4). Solutions of these characteristic equations are

$$\mathrm{sgn}(t)\,\frac{r}{k\,|t|^{\alpha}} = \text{constant}\,, \tag{A9}$$

$$\frac{u}{r^{1-(1/\alpha)}} = \text{constant}\,, \tag{A10}$$

$$\frac{P}{r^{2-(2/\alpha)}} = \text{constant}\,, \tag{A11}$$

$$\rho = \text{constant}\,, \tag{A12}$$

where k is an arbitrary dimensional constant. We set k to unity in the numerical calculations. Equations (A9–A12) are the invariant coordinates of the group generator given by (A1). If we define

$$\xi \equiv \mathrm{sgn}(t)\,\frac{r}{k\,|t|^{\alpha}}\,, \tag{A13}$$

$$v(\xi) \equiv \frac{u}{r^{1-(1/\alpha)}}\,, \tag{A14}$$

$$p(\xi) \equiv \frac{P}{r^{2-(2/\alpha)}}\,, \tag{A15}$$

$$d(\xi) \equiv \rho\,, \tag{A16}$$

then (4–6) may be reformulated as ODEs with the new dependent variables v, p, and d as functions of the new independent variable ξ. Alternatively, (A14–A16) may be nondimensionalized through the transformations

$$V(\xi) \equiv v\,\xi\,k\,, \tag{A17}$$

$$C(\xi) \equiv \gamma\,p\,d\,(\xi k)^2\,, \tag{A18}$$

$$D(\xi) \equiv \frac{d}{\rho_0}\,. \tag{A19}$$

With (A17–A19), (A14–A16) reduce to (18–21). A more rigorous and detailed derivation of (18–21), including an explanation of the meaning of the group generator given in (A1), is provided by Axford and Holm [4,5], Axford [3], and Ramsey [54].

Appendix B: Details of the Numerical Solution Procedure

Here we provide some practically useful computational details omitted from the main text, following Lazarus [36]. First, we explain the differences between Lazarus' method and the method in §3.1. Next, we discuss a few algorithmic details not given in Lazarus' paper. Finally, we discuss alternatives to the methods in §5 for prescribing boundary conditions for Eulerian and Lagrangian compressible flow codes.

The two main differences between Lazarus' method and that in §3.1 are the definitions of the independent similarity variable and the dimensionless sound speed. Instead of the similarity variable ξ, Lazarus uses

$$x \equiv t/r^{\lambda}\,, \tag{B1}$$

where, effectively, $\alpha \equiv 1/\lambda$. The initial condition is imposed at $x = -1$ at time $t = -1$, and x (rather than V, as in (22–24)) is taken as the independent variable. This strategy has the virtue of greatly simplifying the computation of the solution as it passes through focus. Instead of the similarity variable ξ approaching $-\infty$ at this point, the variable x passes smoothly through the origin from negative to positive values. The integration continues up to the reflected shock point $x = B$ (assuming the Lazarus definition of B), where the general jump conditions are imposed. The integration then proceeds to "infinity," i.e., large values of x, which correspond to physical values of r near the origin for $t > 0$. In fact, the point $x = \infty$ is a saddle point; therefore, although V theoretically asymptotes to a constant there (see (37)), it numerically diverges to $\pm\infty$ (roundoff error precludes the numerical calculation from staying on the separatrix). The integration stops when the absolute value of the numerical V becomes "too large." The velocity, sound speed, and density are decomposed as in (19–21), where, e.g., $V(x)$ and $V(\xi)$ now denote different functions (with apologies to the reader for this abuse of notation). The Lazarus methodology also differs through the use of a dimensionless sound speed $\tilde{C}$ that is the square root of the C defined by (20); that is $c(r,t) = r\,\tilde{C}(x)/t$. This alternative definition causes no essential difference, but makes the interpretation of diagrams in the $(V, \tilde{C})$ plane easier to interpret.

With these modifications, it is necessary to integrate only two ODEs for V and $\tilde{C}$, since the third equation for D can then be solved by numerical quadrature. This approach is also attractive because the qualitative theory can be considered in a plane instead of 3-space, and thus is easier to understand. We shall see, however, that it is preferable to integrate all three equations.

There are three singular points. The first singular point, $(V^*, \tilde{C}^*)$ given near (42), occurs before the focus, where the numerators and denominators of the differential equations approach zero. The second singular point is at the focus $x = 0$, where the Lazarus differential equations each contain a factor of x in the denominator. The third is at the point $x = \infty$ or $\xi = 0^+$, which is the aforementioned saddle point. Lazarus discusses the first two points, but does not indicate how to avoid computational difficulties near them.

Near the first point, the two equations behave like $d\tilde{C}/dV = (\tilde{C} - \tilde{C}^*)/(V - V^*)$. The solution of this equation is $c_1\,(\tilde{C} - \tilde{C}^*) = c_2\,(V - V^*)$, where c_1 and c_2 are any

non-zero constants. Locally, any straight line through the point $V = V^*$, $\tilde{C} = \tilde{C}^*$ is a solution. The requirement that $Q = 0$ together with the initial conditions select the proper one.

We consider two approaches to computing in the neighborhoods of the first two singular points. The first is to perform asymptotic expansions in the neighborhoods of each point, as in §4. In this case, an algorithm for switching between the differential equations and the asymptotic expansions must be employed. The second uses no expansions, and directly integrates the differential equations through the singularities. We prefer the second method, as long as we can assess how much accuracy is lost in passing through the singularities.

At this point, the third differential equation becomes useful. We define the total energy (up to a multiplicative constant) as

$$E(x) \equiv \frac{\frac{1}{2} D(x)V^2(x) + D(x)C^2(x)/(\gamma(\gamma-1))}{x^2} . \tag{B2}$$

This energy integral is invariant for all x until the solution trajectory passes through the reflected shock. Monitoring this quantity provides a measure of the solution accuracy near the two singular points. Thus, we define the energy check as $E(x) - E(x = -1)$.

We typically specify the (local) relative error tolerance of the ODE solver at about 10^{-15} (assuming IEEE double precision). By comparing data generated with the ODE solver for successive relative error tolerances of 10^{-j}, $j = 6, 7, \ldots, 16$, we can ascertain that the solutions are accurate to approximately 14 digits. This determination also requires that the rootfinder tolerance for the determination of α be sufficiently tight. We find that the energy check begins at approximately the same figure (i.e., to within an order of magnitude) and remains roughly the same as the integration passes through the first singular point. These results indicate that no accuracy is lost by integrating through this point. In passing through the focus, the energy check increases to about 10^{-11}. This phenomenon suggests that three to four digits of accuracy are lost through focus. As we cannot imagine a situation in which this outcome would not be tolerable, our strategy of not using asymptotic expansions is vindicated. This behavior is qualitatively the same for all cases of m and γ given in Tables 1 and 2.

Finally, we consider alternative methods for prescribing boundary conditions for compressible flow codes. First, we consider Eulerian codes. The result of the ODE integration is a table of $D(x)$, $V(x)$, and $C(x)$ values vs. x from $x = -1$ to $x =$ "infinity." Using the definition of the similarity variable x given in (B1), it is trivial to convert to a table of three physical flow variables versus time from $t = -1$ to $t =$ "infinity" at a fixed position r. If the compressible flow code can accept such a table as input, and automatically interpolate from within that table, then all is well.

For Lagrangian codes, prescribing boundary conditions is more difficult because the outer boundary is not fixed in space. Let $r = R(t)$ be the location of the outer boundary at time t. By the definition of Lagrangian representation, $dR(t)/dt = u(R(t), t) = R(t)\,V(x)/t$. From the definition of the similarity variable, $x = t/R(t)^\lambda$, so x evaluated at the boundary is a function of t only. It can be shown that this function is monotone and thus has an inverse. While it is not possible to compute $R(t)$ directly, it *is* possible to derive an ODE for the function $R(x)$ considered as a function of x (with further apologies to the reader for this additional abuse of notation). Using the chain rule on the Lagrangian definition, we obtain $dR/dt = (dR/dx)(dx/dt) = R(x)\,V(x)/t$. We multiply this equation by dt/dx to obtain a linear equation for dR/dx and dt/dx. Differentiating the similarity variable definition $t = xR(x)^\lambda$ with respect to x yields

a second linear equation for these quantities. This 2×2 linear system can be solved exactly by successive substitutions to yield $dR/dx = R(x)V(x)/[x(1 - \lambda V(x))]$ and $dt/dx = R(x)^{\lambda}/(1 - \lambda V(x))$. The latter confirms that, at least ahead of the reflected shock, t is a monotone function of x, since $V(x)$ is negative there. We observe in practice that x is also monotone elsewhere. We thus obtain an ODE in x for the position of the boundary $R(x)$. Solving this equation requires knowledge of not just R, but also V. If we solve this equation *simultaneously* with the original three ODEs, we can determine $R(x)$ and $t = xR(x)^{\lambda}$ (and have computed the *inverse* function of the position of the boundary). As before, the x table is then converted to a t table, with the three original dependent variables. This approach has been successfully implemented in a research Lagrangian compressible flow code [9], and can also be used for an Arbitrary Lagrangian-Eulerian (ALE) code with the option of forcing the outermost layer of computational cells to "act Lagrangian."

Appendix C: Calculation of Cell-Averaged Values

Appropriate initialization of the compressible flow code using values based on the semi-analytic Guderley solution is extremely important for proper comparison of exact and computed quantities. As the RAGE compressible flow algorithm is based on finite-volume approximations, the quantities it calculates are cell-averaged values. To initialize the code with a non-trivial flow field, one cannot simply use the point-wise flow fields that solve (22–24), as obtained with the procedure described in §3.[7]

In order to provide input consistent with a finite-volume approach, one must evaluate cell-averaged flow fields that are consistent with the exact Guderley solution. Moreover, these cell-averaged values must be constructed from conserved quantities corresponding to those used in the governing conservation laws, namely, mass, momentum, and total energy. For the cell delimited by $r_{\min}$ and $r_{\max}$, we compute the volume $V_{\rm cell}$, mass $M_{\rm cell}$, momentum $MOM_{\rm cell}$, and total energy $E_{\rm cell}$ on a cell-by-cell basis. Using the notation introduced above, these quantities are evaluated as follows:

$$V_{\rm cell} \equiv \frac{S_m}{m} \left(r_{\max}^m - r_{\min}^m \right) \tag{C1}$$

$$M_{\rm cell} \equiv S_m \int_{r_{\min}}^{r_{\max}} dr\, r^{m-1}\, \rho(r)\,, \tag{C2}$$

$$MOM_{\rm cell} \equiv S_m \int_{r_{\min}}^{r_{\max}} dr\, r^{m-1}\, \rho(r)\, u(r)\,, \tag{C3}$$

$$E_{\rm cell} \equiv S_m \int_{r_{\min}}^{r_{\max}} dr\, r^{m-1}\, \rho(r) \left[e(r) + \frac{1}{2} u^2(r) \right], \tag{C4}$$

where m is the space dimension and S_m is the surface area of the unit ball ($S_m = 2$, 2π, or 4π for $m = 1$, 2, or 3, respectively). These quantities were evaluated numerically using the FORTRAN routine DQAGS [47], with the integrand functions obtained from the semi-analytic solution.

[7] Timmes et al. [61] provide a detailed discussion of this issue for another compressible flow problem.

On a cell-by-cell basis, the values used to initialize the compressible flow code are then defined as follows:

$$\rho_{\rm cell} \equiv M_{\rm cell}/V_{\rm cell}\,, \tag{C5}$$

$$u_{\rm cell} \equiv MOM_{\rm cell}/\rho_{\rm cell}\,, \tag{C6}$$

$$e_{\rm cell} \equiv E_{\rm cell}/\rho_{\rm cell} - \frac{1}{2}\left(MOM_{\rm cell}/\rho_{\rm cell}\right)^2\,. \tag{C7}$$

Acknowledgements This work was performed under the auspices of the United States Department of Energy by Los Alamos National Security, LLC, at Los Alamos National Laboratory under contract DE-AC52-06NA25396. SDR and JRK acknowledge the support of the US Department of Energy Advanced Strategic Computing Program Verification Project under project leaders J. Brock and F. Hemez. The authors thank M. Clover, J. Grove, G. Hutchens, W. Rider, F. Timmes, and T. Trucano for valuable insights on these topics.

References

1. Arora, M., Roe, P.: On postshock oscillations due to shock capturing schemes in unsteady flows. J. Comput. Phys. **130**, 25–40 (1997)
2. Atenzi, S., Meyer-ter-Vehn, J.: The Physics of Inertial Fusion. Oxford University Press, New York, USA (2004)
3. Axford, R.: Solutions of the Noh problem for various equations of state using Lie groups. Lasers and Particle Beams **18**, 93–100 (2000)
4. Axford, R., Holm, D.: Spherical shock collapse in a non-ideal medium. In: Proceedings of the Joint IUTAM/IMU Symposium, Group Theoretical Methods in Mechanics, pp. 47–56. ECCOMAS Computational Fluid Dynamics Conference (1978)
5. Axford, R., Holm, D.: Converging finite-strength shocks. Physica D **2**, 194–202 (1981)
6. Benson, D.: Computational methods in Lagrangian and Eulerian hydrocodes. Comp. Meth. Appl. Mech. Engrg. **99**, 235–394 (1992)
7. Bilbao, L., Gratton, J.: Spherical and cylindrical convergent shocks. Nuovo Cimento **18**, 1041–1060 (1996)
8. Bouchut, F.: Nonlinear Stability of Finite Volume Methods for Hyperbolic Conservation Laws and Well-Balanced Schemes for Sources. Birkhäuser Verlag, Basel, Switzerland (2004)
9. Brandon, S.: personal communication (2009)
10. Brushlinskii, K.: Instability of a convergent spherical shock wave. USSR Computational Mathematics and Mathematical Physics **22**, 193–205 (1982)
11. Butler, D.: Converging spherical and cylindrical shocks. Tech. Rep. 54/54, UK Armament Res. Estab. (1954)
12. Chester, W.: The quasi-cylindrical shock tube. Phil. Mag. **45**, 1293–1301 (1954)
13. Chisnell, R.: The motion of a shock wave in a channel, with applications to cylindrical and spherical shock waves. J. Fluid Mech. **2**, 286–298 (1957)
14. Chisnell, R.: An analytic description of converging shock waves. J. Fluid Mech. **354**, 357–375 (1998)
15. Clarisse, J.M.: A Godunov-type method in Lagrangian coordinates for computing linearly-perturbed spherically-symmetric flows of gas dynamics (2007). URL http://hal.archives-ouvertes.fr/hal-00197498
16. Clark, D., Tabak, M.: Isochoric implosions for fast ignition. Tech. Rep. UCRL-CONF-221925, Lawrence Livermore National Laboratory (2006)
17. Coggeshall, S.: Analytic solutions of hydrodynamics equations. Phys. Fluids A **3**, 757–769 (1991)
18. Coggeshall, S., Axford, R.: Lie group invariance properties of radiation hydrodynamics equations and their associated similarity solutions. Phys. Fluids **29**, 2398–2420 (1986)
19. Coggeshall, S., Meyer-ter-Vehn, J.: Group-invariant solutions and optimal systems for multidimensional hydrodynamics. J. Math. Phys. **33**, 3585–3601 (1992)
20. Fernández, M.: Implosiones y Explosiones en Medios Condensados. Ph.D. thesis, Escuela Técnica Superior de Ingenieros Aeronáuticos, Madrid (1977)

21. Fink, M., Hillebrandt, W., Röpke, F.: Double-detonation supernovae of sub-Chandrasekhar mass white dwarfs. Astronomy & Astrophysics **476**, 1133–1143 (2007)
22. Forsythe, G., Malcolm, M., Moler, C.: Computer Methods for Mathematical Computations. Prentice-Hall, Englewood Cliffs, USA (1977)
23. Gittings, M., Weaver, R., Clover, M., Betlach, T., Byrne, N., Coker, R., Dendy, E., Hueckstaedt, R., New, K., Oakes, W., Ranta, D., Stefan, R.: The RAGE radiation-hydrodynamics code. Comput. Sci. Disc. **1**, 015005 (2008)
24. Guderley, G.: Starke kugelige und zylindrische Verdichtungsstöße in der Nähe des Kugelmittelpunktes bzw. der Zylinderachse. Luftfahrtforschung **19**, 302–312 (1942)
25. Gurovich, V., Fel, L.: Landau-Stanyukovich rule and the similarity parameter for converging shocks. JETP Letters **89**, 14–18 (2009)
26. Häfele, W.: Über die Stabilität des Guderleyschen kugeligen Verdichtungsstoßes. Z. Naturforschung **11**, 183–186 (1956)
27. Hafner, P.: Verdichtung und Reaktivitätsaufbau bei der Zündung von Kernspaltungswaffen, Teil 1: Analytische Näherung zum einfallenden Guderleyschen Verdichtungsstoß. Tech. Rep. 109, Fraunhofer-Institut für Naturwissenschaftlich-Technische Trendanalysen (INT) (1982)
28. Hafner, P.: Strong convergent shock waves near the center of convergence: A power series solution. SIAM J. Appl. Math. **48**, 1244–1261 (1998)
29. Hemez, F., Brock, J., Kamm, J.: Non-linear error ansatz models in space and time for solution verification. In: Proceedings of the 47th Structures, Structural Dynamics, and Materials (SDM) Conference and 8th Non-Deterministic Approaches (NDA) Conference. AIAA/ASME/ASCE/AHS/ASC (2006)
30. Hirschler, T.: A parametric study of self-similar collapsing shock waves in radiating gas. Phys. Fluids **14**, 1491–1501 (2002)
31. Hirschler, T., Gretler, W.: On the eigenvalue problem of imploding shock waves. Z. agnew. Math. Phys. **52**, 151–166 (2001)
32. Hornung, H., Pullin, D., Ponchaut, N.: On the question of universality of imploding shock waves. Acta Mech. **201**, 31–35 (2008)
33. Jena, J., Sharma, V.: Self-similar shocks in a dusty gas. Int. J. Non-Linear Mech. **34**, 313–327 (1999)
34. Kamm, J., Rider, W., Brock, J.: Combined space and time convergence analyses of a compressible flow algorithm. Tech. Rep. AIAA-2003-4241, American Institue of Aeronautics and Astronautics (2003)
35. Lazarus, R.: Comments on "Analysis of spherical imploding shocks". Phys. Fluids **23**, 844–844 (1980)
36. Lazarus, R.: Self-similar solutions for converging shocks and collapsing cavities. SIAM J. Numer. Anal. **18**, 316–371 (1981)
37. Lazarus, R.: Erratum: Self-similar solutions for converging shocks and collapsing cavities. SIAM J. Numer. Anal. **19**, 1090–1090 (1982)
38. Lazarus, R., Richtmyer, R.: Similarity solutions for converging shocks. Tech. Rep. LA-6823-MS, Los Alamos Scientific Laboratory (1977)
39. LeVeque, R.: Finite Volume Methods for Hyperbolic Problems. Cambridge University Press, Cambridge, UK (2002)
40. Madhumita, G., Sharma, V.: Propagation of strong converging shock waves in a gas of variable density. J. Engrg. Mech. **46**, 55–68 (2003)
41. Meyer-ter-Vehn, J., Schalk, C.: Selfsimilar spherical compression waves in gas dynamics. Z. Naturforsch. A **37**, 955–969 (1982)
42. Mishkin, E.: Reply to comments by Roger B. Lazarus. Phys. Fluids **23**, 844–846 (1980)
43. Mishkin, E., Fujimoto, Y.: Analysis of a cylindrical imploding shock wave. J. Fluid Mech. **89**, 61–78 (1978)
44. Mishkin, E., Fujimoto, Y.: Analysis of spherically imploding shocks. Phys. Fluids **21**, 1933–1938 (1978)
45. Morawetz, C.: Contracting Spherical Shocks Treated by a Perturbation Method. Ph.D. thesis, New York University (1951)
46. Motz, H.: The Physics of Laser Fusion. Academic Press, New York, USA (1979)
47. Netlib Repository at UTK and ORNL. URL http://www.netlib.org/
48. NiCastro, J.: Similarity analysis of the radiative gas dynamic equations with spherical symmetry. Phys. Fluids **13**, 2000–2006 (1970)
49. Noh, W.: Errors for calculations of strong shocks using an artificial viscosity and an artificial heat flux. J. Comp. Phys. **72**, 78–120 (1987)

50. Oberkampf, W., Trucano, T., Hirsch, C.: Verification, validation, and predictive capability in computational engineering and physics. Appl. Mech. Rev. **57**, 345–384 (2004)
51. Ovsiannikov, L.: Group Analysis of Differential Equations. Academic Press, New York, USA (1982)
52. Ponchaut, N.: Part I: 3DPTV: Advances and Error Analysis. Part II: Extension of Guderleys Solution for Converging Shock Waves. Ph.D. thesis, California Institute of Technology (2005)
53. Ponchaut, N., Hornung, H., Pullin, D., Mouton, C.: On imploding cylindrical and spherical shock waves in a perfect gas. J. Fluid Mech. **560**, 103–122 (2006)
54. Ramsey, S.: A rigorous investigation of the self-similar converging-reflected shock wave standard solution mode. Tech. Rep. LA-UR-07-5261, Los Alamos National Laboratory (2007)
55. Ramsey, S.: Evaluation of the Guderley converging shock wave standard solution mode. Tech. Rep. LA-UR-08-5442, Los Alamos National Laboratory (2008)
56. Rodríguez, M., Amable, L.: Implosiones Autosemejantes Isentropicas y No Isentropicas. Tech. Rep. J.E.N. 405, Junta de Energía Nuclear (1978)
57. Roy, C.: Review of code and solution verification procedures for computational simulation. J. Comput. Phys. **205**, 131–156 (2005)
58. Rygg, J.: Shock Convergence and Mix Dynamics in Inertial Confinement Fusion. Ph.D. thesis, Massachusetts Institute of Technology (2006)
59. Sedov, L.: Similarity and Dimensional Methods in Mechanics. Academic Press, New York, USA (1959)
60. Stanyukovich, K.: Unsteady Motion of Continuous Media. Pergammon Press, New York, USA (1970)
61. Timmes, F., Clover, M., Kamm, J., Ramsey, S.: On a cell-averaged solution to the Coggeshall #8 problem. Tech. Rep. LA-UR-09-04438, Los Alamos National Laboratory (2009)
62. Toqué, N.: Self-similar implosion of a continuous stratified medium. Shock Waves **11**, 157–165 (2001)
63. Van Dyke, M., Guttmann, A.: The converging shock wave from a spherical or cylindrical piston. J. Fluid Mech. **120**, 451–462 (1982)
64. Wang, J.: On the theory of imploding shocks. J. Appl. Math. Physics **33**, 53–62 (1982)
65. Whitham, G.: On the propagation of shock waves through regions of non-uniform area or flow. J. Fluid Mech. **4**, 337–360 (1958)
66. Wu, C., Roberts, P.: Structure and stability of a spherical shock wave in a Van der Waals gas. Q. J. Mech. Appl. Math. **49**, 501–543 (1996)
67. Yousaf, M.: Imploding spherical and cylindrical shocks. Phys. Fluids **29**, 680–684 (1986)
68. Zel'dovich, Ya., Raizer, Yu.: Physics of Shock Waves and High-Temperature Hydrodynamic Phenomena. Dover Publications, Mineola, USA (2002)

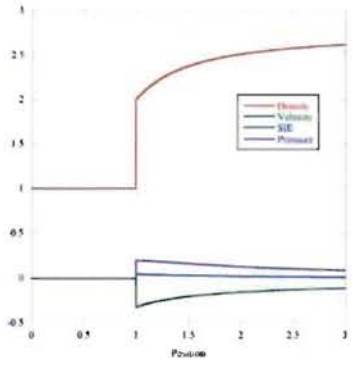

Fig. 1 Semi-analytic solution of the Guderley problem at initialization time $t = -1$, depicting cell-averaged quantities for 1200 cells between $r = 0$ and $r = 3$.

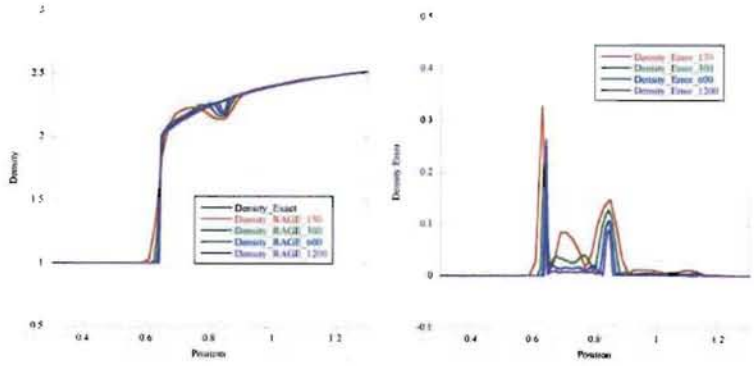

Fig. 2 Left: Semi-analytic and computed Guderley density field at $t = -0.5$. Right: Corresponding pointwise errors. In these plots, the semi-analytic solution is a black line, and the corresponding computed values are colored lines according to the legend.

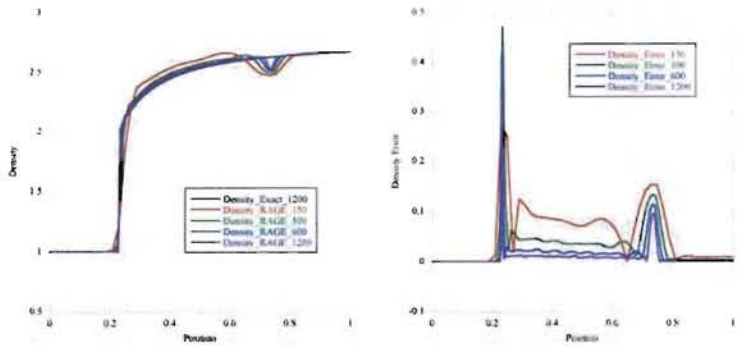

Fig. 3 Left: Semi-analytic and computed Guderley density field at $t = -0.1$. Right: Corresponding pointwise errors.

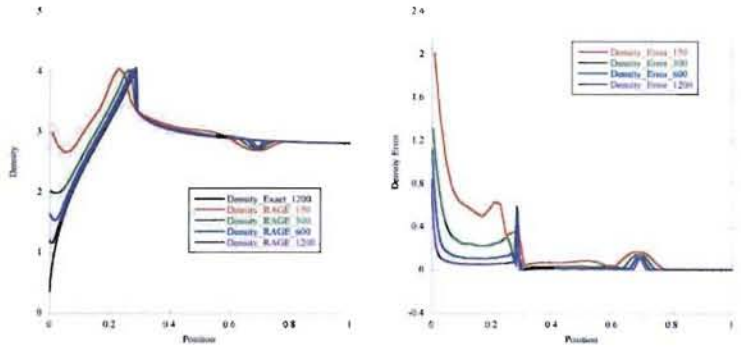

Fig. 4 Left: Semi-analytic and computed Guderley density field at $t = 0.1$. Right: Corresponding pointwise errors.

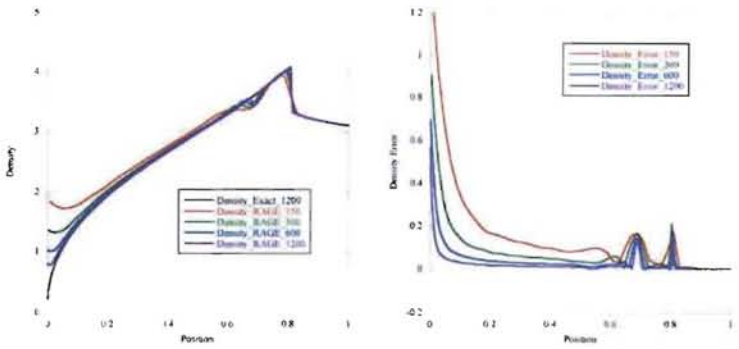

Fig. 5 Left: Semi-analytic and computed Guderley density field at $t = 0.5$. Right: Corresponding pointwise errors.

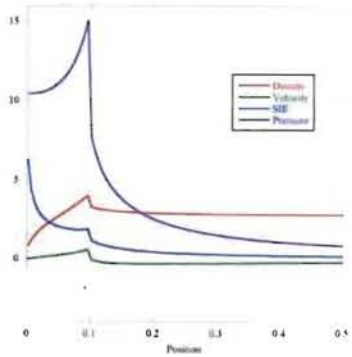

Fig. 6 Semi-analytic solution of the Guderley problem at initialization time $t = 0.018594543$, depicting cell-averaged quantities for 1200 cells between $r = 0$ and $r = 3$.

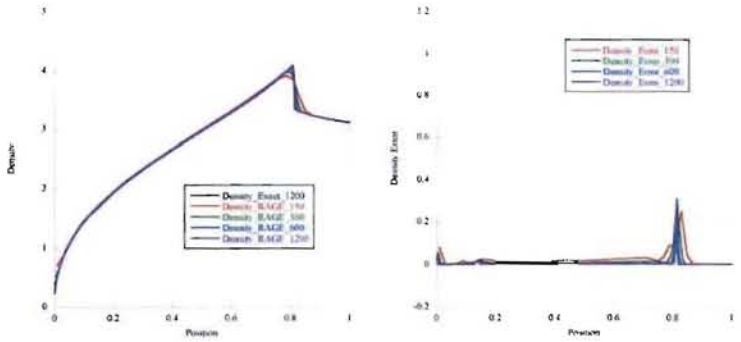

Fig. 7 Left: Semi-analytic and computed Guderley density field at $t = 0.5$, computed from the initial conditions in Fig. 6. Right: Corresponding pointwise errors.

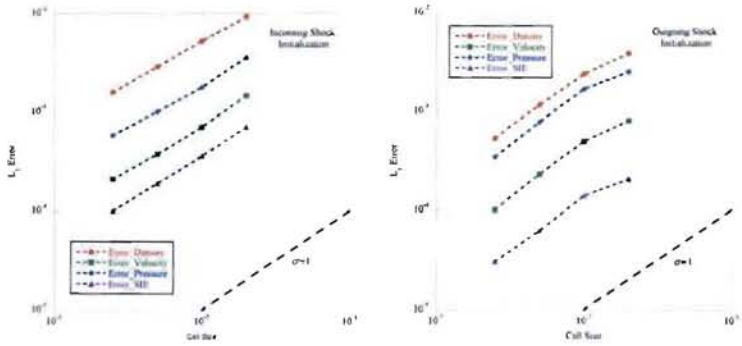

Fig. 8 L_1 errors on $0 \leq r \leq 2$ for flow quantities calculated for the Guderley problem at time $t = 0.5$. Left: Problem initiated with incoming shock wave. Right: Problem initiated with outgoing shock wave. The dashed black line in each plot is a reference line for first-order convergence.